

# Energetic elasticity models for soft biological tissue: Role of the elastica

K. Garikipati, S. Göktepe & C. Miehe

June 16, 2019

## Abstract

Continuum strain energy functions are developed for soft biological tissues that possess long fibrillar components. The treatment is based on the model of an elastica, which is our fine scale model, and is homogenized in a simple fashion to obtain a continuum strain energy function. Notably, we avoid solving the full fourth-order, nonlinear, partial differential equation for the elastica by resorting to other assumptions, kinematic and energetic, on the response of the individual, elastica-like fibrils.

## 1 Background

Strain energy functions for currently-used soft biological tissue have two main origins. Some have been adopted from the rubber elasticity and polymer elasticity literature, and others have functional forms that have been chosen to reproduce the characteristic locking behavior observed in experiments (Holzapfel and Ogden, 2006). Among the rubber/polymer elasticity models are micromechanically-derived ones, which mostly incorporate entropic elasticity (Landau and Lifshitz, 1951). Such models work well for rubber and polymers in which the uncoiling of long chain molecules under axial force causes a decrease in configurational entropy as fewer configurations become available to the molecule that is vibrating due to its thermal energy. However, the applicability of such ideas of entropic elasticity is not clear for many soft biological tissues, such as tendons, ligaments and muscles. As an example, consider the case of tendons, which have a high collagen content. Sun et al. (2002) demonstrated by laser trap experiments that the elasticity of the collagen molecule, which is a triple helix with a diameter of 1.5 nm and a contour length (fully uncoiled length) of  $\approx 300$  nm is well-represented by the worm-like chain model of Kratky and Porod (1949).

However, collagen in tendons is not restricted to the form of long chain molecules in the entirety of the tendon. It forms fibrils of around 300 nm diameter, and lengths of the order of 100s of  $\mu\text{m}$ . These are further ordered into fibers that can run the entire length of tendons (the order of cm). The entire hierarchical structure has extensive crosslinking, including a longitudinal staggering of the collagen molecules that leads to a characteristic banded structure on the scale of a fibril, and a “crimp” in the fibers with a wavelength of  $10 - 50 \mu\text{m}$ . (Screen et al., 2003; Provenzano and Vanderby, 2006). Given this ordered, hierarchical structure with extensive crosslinking, it seems appropriate to question the use of entropic elasticity. It seems unlikely that the collagen molecules have many configurations available to them due to kinematic constraints imposed by the crosslinking. Similar arguments can be made for ligaments and muscles. Some support for this view may be inferred from experiments of Woo et al. (1987). Strain-controlled, cyclic

tension tests of canine medial collateral ligaments at temperatures between 2° C and 37° C showed that the area of hysteresis loops decreased as the temperature of the experiment increased. The strain-control in these experiments implies that the initial modulus of the stress-strain response was decreasing with an increase in temperature. (The standard solid viscoelastic model specifies that the viscosity has no influence on the initial modulus.) This decrease in elasticity with increase in temperature is a signature of energetic elasticity, not entropic elasticity. In fact, entropic elasticity makes the initial modulus increase with temperature, as is well-known Treloar (1975).

One reason for the attractiveness of entropic elasticity models lies in the fact that they reproduce the locking behavior of soft biological tissue in uniaxial tension. However, here it is shown that this characteristic behavior can equally-well be modelled by an energetic model of elasticity that accounts for the uncoiling of crimped fibrils with increasing tension. In this sense, the locking behavior is determined by an elastica-like response of the individual fibrils. This consideration leads to a micromechanically-driven strain energy function for soft tissue, that, as argued above, has the proper basis in energetic elasticity, rather than entropy effects, which are suppressed due to crosslinking.

## 2 The stress-strain response of an elastica

Consider a curve,  $\Gamma$ , in  $\mathbb{R}^3$  parameterized by its arc length,  $S$ , in the reference (undeformed) configuration (Figure 1). Points along the curve are identified by position vectors  $\mathbf{X}(S) \in \mathbb{R}^3$ . The tangent at  $S$  is  $\mathbf{T}(S) = d\mathbf{X}/dS$ . Using a Cartesian basis of orthonormal unit vectors  $\{\mathbf{e}_1, \mathbf{e}_2, \mathbf{e}_3\}$  it is clear that  $dX_I/dS = \cos\alpha_I$ , where  $\alpha_I$ ,  $I = 1, 2, 3$ , is the corresponding direction cosine. It follows that  $\|\mathbf{T}\| = 1$ . The curvature of  $\Gamma$  is  $\kappa_0 = \sqrt{\sum_I (d^2X_I/dS^2)^2}$ . In the deformed configuration,  $\gamma$ , points have position vectors  $\mathbf{x}(S) = \mathbf{X}(S) + \mathbf{u}(S)$ . The tangent vector to  $\Gamma$  is carried to  $\mathbf{t}(S) = d\mathbf{x}/dS$ , and by the chain rule it can be written as

$$\mathbf{t} = \frac{\partial \mathbf{x}}{\partial \mathbf{X}} \frac{d\mathbf{X}}{dS}.$$

Introducing the deformation gradient tensor,  $\mathbf{F} := \partial\mathbf{x}/\partial\mathbf{X}$ , gives  $\mathbf{t} = \mathbf{F}\mathbf{T}$ , from which it follows that  $\|\mathbf{t}\|^2 = \mathbf{T} \cdot \mathbf{C}\mathbf{T}$ , where  $\mathbf{C} = \mathbf{F}^T\mathbf{F}$  is the right Cauchy-Green tensor. The stretch along  $S$  will be denoted by  $\lambda^2 = \|\mathbf{t}\|^2$ , and satisfies  $0 < \lambda^2$ . As an aside, note that if the arc length in the deformed configuration, say  $s$ , is used to parametrize  $\mathbf{x}$  as  $\mathbf{x}(s)$ , then the tangent with respect to  $\gamma$ , which we will denote by,  $\mathbf{t}^\#$  is  $\mathbf{t}^\# = dx/ds$ , and satisfies  $\|\mathbf{t}^\#\|^2 = 1$ . The curvature of  $\gamma$  is  $\kappa = \sqrt{\sum_I (d^2x_I/ds^2)^2}$ , and can be written as  $\kappa = \sqrt{\sum_I (d^2x_I/\lambda^2 dS^2)^2}$ .

The strain energy of  $\Gamma$  is assumed to be decomposed into bending and stretching components,  $W(\kappa, \lambda; \kappa_0) = K(\kappa; \kappa_0) + U(\lambda)$ . For simplicity, we assume that  $\Gamma$  possesses constant bending stiffness  $B$  and stretching modulus  $E$ , cross-sectional area  $A(S, \lambda)$ , and reference contour length  $L$ , such that

$$K(\kappa; \kappa_0) = \int_0^L \frac{1}{2} B(\kappa - \kappa_0)^2 dS, \quad U(\lambda) = \int_0^L \frac{1}{2} EA(\lambda^2 - 1)^2 dS. \quad (1)$$

The governing partial differential equation for the deformation of the elastica is obtained by imposing stationarity of the following Gibbs free energy functional:

$$\mathcal{G}[\mathbf{u}] = \int_0^L \left( \frac{1}{2} B \left( \left\| \frac{d^2\mathbf{x}}{ds^2} \right\| - \kappa_0(S) \right)^2 + \frac{1}{2} EA \left( \left\| \frac{d\mathbf{x}}{dS} \right\|^2 - 1 \right)^2 \right) dS - \int_0^L \mathbf{q} \cdot \mathbf{u} dS - \mathbf{f}(0) \cdot \mathbf{g}(0) - \mathbf{f}(L) \cdot \mathbf{g}(L)$$

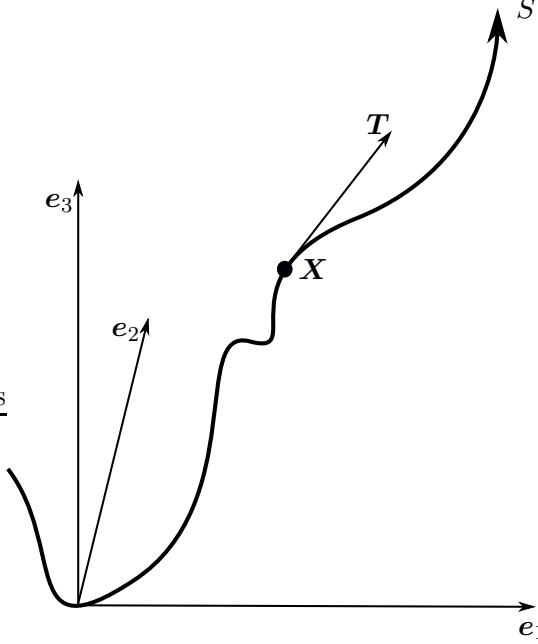


Figure 1: The curve,  $\Gamma \in \mathbb{R}^3$ .

Introducing the variations  $\mathbf{x}_\varepsilon = \mathbf{X} + \mathbf{u} + \varepsilon \mathbf{w}$ , where  $\varepsilon \in \mathbb{R}$ , and  $\mathbf{w}$  is an arbitrary vector field, satisfying  $\mathbf{w}(S) = \mathbf{0}$  at  $S = \{0, L\}$ , the stationarity condition is

$$\frac{d}{d\varepsilon} \mathcal{G}[\mathbf{u}_\varepsilon] = \frac{d}{d\varepsilon} \left( \int_0^L \left( \frac{1}{2} B \left( \left\| \frac{d^2 \mathbf{x}_\varepsilon}{ds^2} \right\| - \kappa_0(S) \right)^2 \frac{1}{2} EA \left( \left\| \frac{d\mathbf{x}_\varepsilon}{ds} \right\|^2 - 1 \right)^2 \right) ds - \int_0^L \mathbf{q} \cdot \mathbf{u}_\varepsilon ds - \mathbf{f}(0) \cdot \mathbf{g}(0) - \mathbf{f}(L) \cdot \mathbf{g}(L) \right)$$

Standard variational calculus, the arbitrariness of  $\mathbf{w}$  and  $d\mathbf{w}/dS$ , as well as the homogeneity of  $\mathbf{w}$  at  $S = 0$  and  $S = L$ , yield the following Euler-Lagrange equations:

$$B \frac{d^2}{\lambda d(\lambda dS)} \left( (1 - \kappa_0/\kappa) \frac{d^2 \mathbf{x}}{\lambda d(\lambda dS)} \right) - 2EA \frac{d}{dS} \left( (\lambda^2 - 1) \frac{d\mathbf{x}}{dS} \right) - \mathbf{q} = 0, \quad (2)$$

with the boundary conditions

$$\mathbf{u} = \mathbf{g} \text{ at } \{0, L\}, \quad B \left( 1 - \frac{\kappa}{\kappa_0} \right) \frac{d^2 \mathbf{x}}{\lambda d(\lambda dS)} = 0 \text{ at } \{0, L\}. \quad (3)$$

Note that boundary conditions on  $\mathbf{u}$  have been assumed at  $S = \{0, L\}$ , and that the generalized force (“moment”) is assumed to vanish at  $S = \{0, L\}$ . Alternate boundary conditions can be used, and are obtained from the above variational procedure.

The ultimate aim of this work is the development of a macroscopic strain energy function, where the micromechanics arises from the deformation of the elastica. The *exact* micromechanics of the deforming elastica is obtained by solving the partial differential equation (2) subject to (3). In order to avoid the complexity and expense of solving this nonlinear, fourth-order partial differential equation repeatedly, we examine certain assumptions, kinematic and otherwise, which simplify the micromechanics. In Section 3 we make the kinematic assumption that the elastica is constrained to remain the arc of a circle. In Section 4 the deforming elastica is constrained to maintain a sinusoidal waveform.

### 3 Force-displacement response of an elastica constrained to the arc of a circle

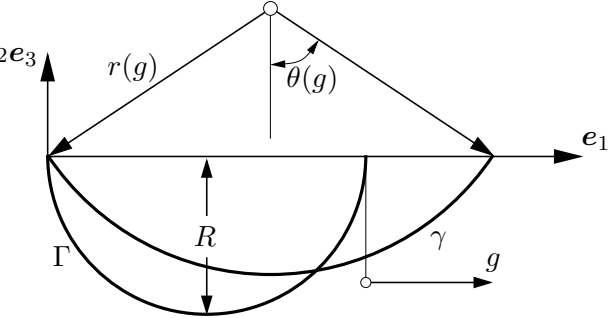


Figure 2: Uncoiling of an initially semi-circular elastica.

Consider an elastica with semicircular reference configuration,  $\Gamma$ , of radius  $R$ , as shown in Figure 2. The reference positions are

$$\mathbf{X}(S) = \begin{Bmatrix} R(1 - \cos(S/R)) \\ 0 \\ -R \sin(S/R) \end{Bmatrix} \quad (4)$$

In this section we explore the effect of further constraints on this deforming elastica. These are the constraints of (i) inextensibility, (ii) incompressibility of the bounding medium, and (iii) energy minimization. In each case, the constraint makes it possible to obtain final deformed shapes without solving the differential equation (2). It is remarked, at the outset, that the constraints considered here are not exhaustive. However, the physical interpretations and motivations are transparent.

#### 3.1 The inextensible elastica constrained to a circular arc

If the point  $S = \pi R$  is displaced by the vector  $g e_1$  while the deformed configuration,  $\gamma$  maintains the form of an inextensible ( $\lambda = 1$ ) circular arc, then the tip displacement is restricted as  $0 \leq g \leq (\pi - 2)R$ . The deformed radius,  $r(g)$ , then satisfies the implicit relation

$$r(g) \sin(\theta(g)) = R + \frac{g}{2} \quad (5)$$

where  $\theta(g) := \pi R / (2r(g))$  as denoted in Figure 2, and the positions of points on  $\gamma$  are

$$\mathbf{x}(S) = \begin{Bmatrix} R + \frac{g}{2} - r \sin(\theta - \frac{S}{r}) \\ 0 \\ r(\cos \theta - \cos(\theta - \frac{S}{r})) \end{Bmatrix}. \quad (6)$$

This gives,

$$\frac{d^2 \mathbf{X}}{dS^2} = \begin{Bmatrix} \frac{1}{R} \cos(\frac{S}{R}) \\ 0 \\ \frac{1}{R} \sin(\frac{S}{R}) \end{Bmatrix}, \quad \frac{d\mathbf{x}}{dS} = \begin{Bmatrix} \cos(\theta - \frac{S}{r}) \\ 0 \\ -\sin(\theta - \frac{S}{r}) \end{Bmatrix}, \quad \frac{d^2 \mathbf{x}}{dS^2} = \begin{Bmatrix} \frac{1}{r} \sin(\theta - \frac{S}{r}) \\ 0 \\ \frac{1}{r} \cos(\theta - \frac{S}{r}) \end{Bmatrix}, \quad (7)$$

from which it follows that  $\kappa_0^2 = 1/R^2$ ,  $\kappa^2 = 1/r^2$  and  $\lambda^2 = 1$ . Note that, for brevity, the dependences  $r(g)$  and  $\theta(g)$  have been suppressed in both (6) and (7) and the limiting case  $g = (\pi - 2)R$ ,  $\gamma$  is a straight segment of length  $\pi R$  along  $\mathbf{e}_1$ .

The strain energy of the elastica can now be written, following (1) as

$$W(\kappa; g) = \int_0^{\pi R} \frac{1}{2} B (\kappa(g) - \kappa_0)^2 dS, \quad 0 \leq g \leq (\pi - 2)R \quad (8)$$

Note that  $W(\kappa; g)$  is a functional of the field,  $\kappa$ , and a function of the tip displacement,  $g$ . The force response of the elastica to the tip displacement,  $g$  is

$$f(\kappa; g) = \frac{dW}{dg}, \quad 0 \leq g \leq (\pi - 2)R \quad (9)$$

Like  $W$ , the force,  $f$  is a functional of  $\kappa$  and a function of  $g$ . In what follows, the functional character of  $f$  is suppressed since its dependence on  $g$  is of primary interest. Using (8) we have,

$$f = \frac{B\pi R}{2r(g)^2} \left( \frac{1}{r(g)} - \frac{1}{R} \right) \frac{1}{\theta \cos \theta - \sin \theta}, \quad 0 \leq g \leq (\pi - 2)R. \quad (10)$$

Equation (10) indicates that  $f(g)$  diverges as  $1/r(g) \rightarrow 0$ . Thus the force in a fully uncoiled, inextensible elastica diverges. The case in which axial tension develops due to stretching along the tangent as the elastica is uncoiled, will be developed in the next section.

### 3.2 The elastica constrained to a circular arc and subject to a macroscopic incompressibility constraint

Collagen fibrils in soft tissues are surrounded by proteoglycan molecules that bind water. At the levels of stress that the tissue is subject to, the proteoglycan matrix is nearly incompressible. Motivated thus, we consider the deforming fibril constrained to lie within a circumscribing cylinder. For the model of an elastica deforming as the arc of a circle in the  $\{\mathbf{e}_1, \mathbf{e}_3\}$  plane we require the invariance of the area of a circumscribing rectangle, even as the rectangle's aspect ratio varies with tip displacement,  $g$ . See Figure 3. The conservation of the area, then, leads us to a closed-form expression for the height,  $a$ , of the current rectangle

$$A_0 \equiv A \quad \rightsquigarrow \quad a(g) = \frac{2R^2}{2R + g}. \quad (11)$$

Having the explicit form of  $a(g)$ , the radius of the deforming elastica can be readily determined from the geometry of Figure 3 as  $r^2 = (r - a)^2 + (R + g/2)^2$ . This yields

$$r(g) = \frac{1}{2} \left( a + \frac{R^4}{a^3} \right). \quad (12)$$

The current curvature  $\kappa(g)$  and stretch  $\lambda(g)$  of the circular elastica then immediately follow

$$\kappa(g) = \frac{1}{r} \quad \text{and} \quad \lambda(g) = \frac{2r\theta}{\pi R} \quad (13)$$

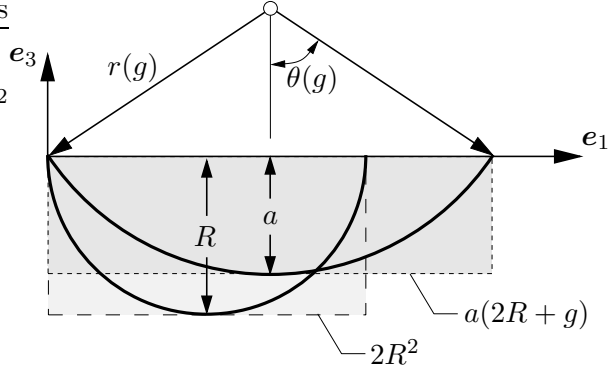


Figure 3: A circular elastica surrounded by an incompressible medium.

where  $\theta(g) := \sin^{-1}((R+g/2)/r(g))$ , see also Figure 3. The inextensibility constraint now does not hold:  $\lambda(g) \neq 1$ . Notice that in both (12) and (13), functional dependencies of  $r(g)$  and  $a(g)$  are suppressed. The strain energy is

$$\overline{W}(g) = \int_0^{\pi R} \frac{1}{2} B (\kappa(g) - \kappa_0)^2 dS + \int_0^{\pi R} \frac{1}{2} EA \left( \left( \frac{2r(g)\theta}{\pi R} \right)^2 - 1 \right)^2 dS \quad (14)$$

For the selected form of the strain energy, we obtain the explicit form of the tip force  $f(g) = d\overline{W}/dg$

$$\begin{aligned} f(g) &= B\pi R \left( \frac{1}{r} - \frac{1}{R} \right) \left( -\frac{1}{4r^2} \right) \left( \frac{3R^2}{a^2} - \frac{a^2}{R^2} \right) \\ &+ 2EA\lambda(\lambda^2 - 1) \left( \frac{1}{\cos\theta} + \frac{\theta - \tan\theta}{2} \left( \frac{3R^2}{a^2} - \frac{a^2}{R^2} \right) \right), \end{aligned} \quad (15)$$

where results of the derivative formulas  $dr/dg = (3R^2/a^2 - a^2/R^2)/4$ ,  $d\kappa/dg = -(1/r^2)dr/dg$  and  $d\lambda/dg = (1/\cos\theta + 2(\theta - \tan\theta)dr/dg)/(\pi R)$  are incorporated.

### 3.3 The deforming elastica constrained to a circular arc, and relaxing to a stationary energy configuration

Referring to Figure 2, and assuming the stretch to be uniformly distributed along the reference contour length gives

$$\lambda = \frac{r(g)\theta(g)}{\pi R/2} \quad (16)$$

where  $\theta(g) := \sin^{-1}((R+g/2)/r(g))$ . Using this result and  $\kappa(g) = 1/r(g)$ ,  $\kappa_0 = 1/R$  in (8) gives the following strain energy function for the elastica

$$\widetilde{W}(r, g) = \int_0^{\pi R} \frac{1}{2} B \left( \frac{1}{r(g)} - \frac{1}{R} \right)^2 dS + \int_0^{\pi R} \frac{1}{2} EA \left( \left( \frac{r(g)}{\frac{\pi}{2}R} \sin^{-1} \left( \frac{g}{2R} \right) \right)^2 - 1 \right)^2 dS. \quad (17)$$

For a given tip displacement,  $g$ , corresponding to an applied force,  $f$ , the constraint that the deformed configuration remains the arc of a circle is now supplemented by requirement that the

deformed radius  $r(g)$  corresponds to the minimum energy state of the elastica. The radius,  $r(g)$ , is the solution of the following minimization condition:

$$\frac{\partial \widetilde{W}}{\partial r} = B\pi R \left( \frac{1}{R} - \frac{1}{r} \right) \frac{1}{r^2} + 4EA\lambda(\lambda^2 - 1)(\theta - \tan \theta) = 0. \quad (18)$$

With the deformed radius thus known, the force is

$$f = \frac{\partial \widetilde{W}}{\partial g} = 2EA\lambda \frac{\lambda^2 - 1}{\cos \theta}. \quad (19)$$

Note that the extension of the above results (10), (15) and (19) for half-wavelengths to an elastica whose waveform consists of  $n$  such half-wavelengths (Figure 4) is straightforward. By symmetry, the force,  $f$ , that results in a total tip displacement of  $g$  corresponds to an extension of  $g/n$  of each half-wavelength, and is obtained from (10), (15) or (19) by substituting  $g$  with  $g/n$ .

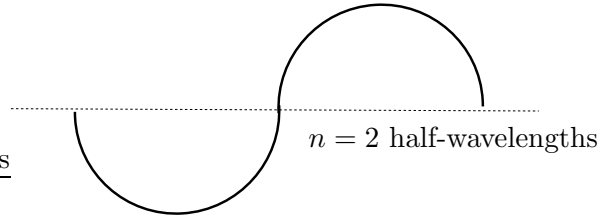


Figure 4: An elastica in which the reference configuration waveform consists of half-wavelengths that are semi-circles.

## 4 The force-displacement response of a sinusoidal elastica

For the sinusoidal waveform, the reference configuration of the elastica is defined by two shape parameters, the amplitude  $a_0$  and the half-wave length  $l_0$ , see Figure 5. As in Section 3 the elastica

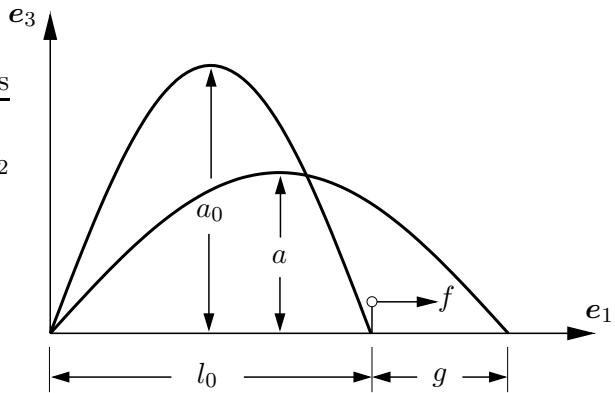


Figure 5: Uncoiling of a sinusoidal elastica.

is constrained to the  $\{e_1, e_2\}$  plane. The reference coordinates of the points on the elastica can be expressed by a single parameter  $t$ , as

$$\mathbf{X}(t) = \begin{Bmatrix} X_1(t) \\ 0 \\ X_3(t) \end{Bmatrix} = \begin{Bmatrix} t \\ 0 \\ a_0 \sin\left(\frac{\pi}{l_0}t\right) \end{Bmatrix} \quad (20)$$

where  $t \in [0, l_0]$ . Analogously, the shape of a deformed elastica can also be formulated in terms of another spatial parameter  $\tilde{t}$ ,

$$\mathbf{x}(\tilde{t}) = \begin{Bmatrix} x_1(\tilde{t}) \\ 0 \\ x_3(\tilde{t}) \end{Bmatrix} = \begin{Bmatrix} \tilde{t} \\ 0 \\ a \sin\left(\frac{\pi}{l}\tilde{t}\right) \end{Bmatrix} \quad (21)$$

where all  $\tilde{t} \in [0, l]$ . The value of the current half-wavelength  $l$  is determined by the tip displacement  $g$  through the relation  $l := l_0 + g$ . This definition immediately implies a linear relation between the Eulerian  $\tilde{t}$  and Lagrangian  $t$  parameters

$$\tilde{t} := t l/l_0 = t (1 + g/l_0) \quad \text{and} \quad \partial_t \tilde{t} = l/l_0 = (1 + g/l_0). \quad (22)$$

With this relation at hand, we can further deduce that the argument of the sine functions appearing in both (20) and (21) have the same value, i.e.

$$\alpha(t) := \frac{\pi}{l_0} t = \frac{\pi}{l} \tilde{t}. \quad (23)$$

This geometrical description of the problem allows us to introduce the two main kinematic variables, namely the curvature,  $\kappa$ , and the stretch,  $\lambda$ , as functions of derivatives of  $X_3$  and  $x_3$  with respect to the Lagrangian  $t$  and the Eulerian  $\tilde{t}$  parameters, respectively. For the planar reference and current curves parameterized by the parameters  $t$  and  $\tilde{t}$ , the general curvature formulas given in Section 2 can be simplified to the forms

$$\kappa_0(t) := \frac{X_3''}{(1 + X_3'^2)^{3/2}}, \quad \kappa(\tilde{t}) := \frac{x_3''}{(1 + x_3'^2)^{3/2}}. \quad (24)$$

The superscript  $(\cdot)'$  in (24) denotes the derivatives

$$\begin{aligned} X_3' &:= \frac{\partial X_3}{\partial t} = a_0 \frac{\pi}{l_0} \cos(\alpha(t)), & X_3'' &:= \frac{\partial^2 X_3}{\partial t^2} = -a_0 \frac{\pi^2}{l_0^2} \sin(\alpha(t)), \\ x_3' &:= \frac{\partial x_3}{\partial \tilde{t}} = a \frac{\pi}{l} \cos(\alpha(t)), & x_3'' &:= \frac{\partial^2 x_3}{\partial \tilde{t}^2} = -a \frac{\pi^2}{l^2} \sin(\alpha(t)). \end{aligned} \quad (25)$$

In this framework, the local value of stretch can be calculated by  $\lambda := ds/dS$  where the infinitesimal arc length measures  $dS$ , and  $ds$  are defined by  $dS := \sqrt{dX_1^2 + dX_3^2} = \sqrt{1 + X_3'^2} dt$  and  $ds := \sqrt{dx_1^2 + dx_3^2} = \sqrt{1 + x_3'^2} d\tilde{t}$ , respectively. Then, combining these results with the one given in (22)<sub>2</sub> yields the stretch expression

$$\lambda := ds/dS = \frac{\sqrt{1 + x_3'^2}}{\sqrt{1 + X_3'^2}} \frac{l}{l_0}. \quad (26)$$

Having the basic kinematic variables  $\kappa_0$ ,  $\kappa$  and  $\lambda$  defined, the overall energy of the sinusoidal elastica in the reference configuration is specified to be

$$\tilde{W}(g; a(g)) = \int_0^{l_0} \frac{1}{2} B(\kappa(t, g; a(g)) - \kappa_0(t))^2 J(t) dt + \int_0^{l_0} \frac{1}{2} EA(\lambda^2(t, g; a(g)) - 1)^2 J(t) dt \quad (27)$$

where  $J(t) := dS/dt = \sqrt{1 + X_3'^2}$ . The tip force  $f(g)$  being energy-conjugate to the tip displacement  $g$  is then given by

$$f(g) = \frac{d\tilde{W}(g; a(g))}{dg} = \left. \frac{\partial \tilde{W}(g; a(g))}{\partial g} \right|_{a(g)} + \left. \frac{\partial \tilde{W}(g; a(g))}{\partial a} \right. \frac{da(g)}{dg} \quad (28)$$

or

$$\begin{aligned} f(g) &= \int_0^{l_0} B(\kappa(t, g; a(g)) - \kappa_0(t)) \frac{d\kappa(t, g; a(g))}{dg} J(t) dt \\ &+ \int_0^{l_0} EA(\lambda^2(t, g; a(g)) - 1) \frac{d\lambda^2(t, g; a(g))}{dg} J(t) dt. \end{aligned} \quad (29)$$

In order to complete the geometrical and constitutive description of the deforming sinusoidal elastica, we need to calculate the value of the spatial amplitude  $a$  for a given tip displacement  $g$ . Apart from the main kinematic assumption that the deforming elastica maintains its sinusoidal shape, an additional constraint is required, as in the case of the elastica deforming as a circular arc. In the case of the sinusoidal elastica, the additional constraint determines the current amplitude  $a$ . As in Section 3 we consider the same the three possible formulations will be considered in the subsequent part of the section. These are based on the constraints concerning: constraints of (i) inextensibility, (ii) incompressible bounding medium, and (iii) energy minimization.

#### 4.1 Force-displacement response of an inextensible sinusoidal elastica

The local inextensibility condition requires that  $\lambda := ds/dS = 1$  and thus

$$\lambda^2 - 1 = \frac{1 + x_3'^2 l^2}{1 + X_3'^2 l_0^2} - 1 = 0. \quad (30)$$

Inserting the results in (36)<sub>1</sub> and (38)<sub>1</sub> into (30), yields expression for the square of the current amplitude  $a$

$$a^2 = a_0^2 - \frac{l^2 - l_0^2}{\pi^2 \cos^2(\alpha)}. \quad (31)$$

It is apparent from the expression (31) that  $a^2$  diverges towards  $-\infty$  in the limit  $\alpha \rightarrow \pi/2$ . Even for positive values of  $a^2$ , the amplitude will vary along the curve disturbing the sinusoidal shape of the elastica. Therefore, we impose the inextensibility constraint in a global sense, by enforcing conservation of the length of a sinusoidal elastica for a given tip displacement  $g$ :

$$\int_s ds = \int_S dS \quad \leadsto \quad \int_0^{l_0} (\lambda(t, g; a) - 1) J(t) dt = 0. \quad (32)$$

This condition defines a non-linear residual

$$\mathcal{R}(a) := \int_0^{l_0} (\lambda(t, g; a) - 1) J(t) dt = 0 \quad (33)$$

that must be solved for the current amplitude  $a$  satisfying the global inextensibility condition for a given constant tip displacement  $g$ . In order to solve this non-linear residuum a Newton-type iterative scheme must be employed. We linearize the residual  $\mathcal{R}(a)$  about  $a = \bar{a}$ ,  $\text{Lin } \mathcal{R}(a)|_{\bar{a}} := \mathcal{R}(\bar{a}) + (\partial \mathcal{R}/\partial a)|_{\bar{a}}(a - \bar{a}) = 0$ , and solve this equation for  $a$  to get  $a = \bar{a} - \mathcal{R}(\bar{a})/(\partial \mathcal{R}/\partial a)|_{\bar{a}}$ . For each given value of tip displacement  $g$ , this iterative update scheme is repeated until iterates for  $a$  converge to within a tolerance. Once the value of  $a$  is computed, we can continue with the computation of the tip force  $f$ . To this end, we need the sensitivity of the amplitude  $a(g)$  to the

tip displacement  $g$ . It can be calculated by exploiting the implicit form of the residual  $\mathcal{R}(g; a(g))$  for a general displacement controlled loading process by writing  $d\mathcal{R}(g; a(g))/dg = (\partial\mathcal{R}/\partial g)|_a + (\partial\mathcal{R}/\partial a)(\partial a/\partial g) = 0$  yielding  $\partial a/\partial g = -(\partial\mathcal{R}/\partial g)/(\partial\mathcal{R}/\partial a)$ . Having this sensitivity at hand, we can now proceed with the computation of the integrands appearing in the force expression (29)

$$\begin{aligned}\frac{d\kappa}{dg} &= \frac{\partial\kappa}{\partial g}\Big|_a + \frac{\partial\kappa}{\partial a}\Big|_g \frac{da}{dg} = \frac{x_3''}{(1+x_3'^2)^{5/2}} \left( \frac{(x_3'^2-2)}{l} + \frac{(1-2x_3'^2)}{a} \frac{da}{dg} \right), \\ \frac{d\lambda^2}{dg} &= \frac{\partial\lambda^2}{\partial g}\Big|_a + \frac{\partial\lambda^2}{\partial a}\Big|_g \frac{da}{dg} = \frac{2l}{l_0^2(1+X_3'^2)} \left( 1 + x_3'^2 \frac{l}{a} \frac{da}{dg} \right).\end{aligned}\quad (34)$$

## 4.2 Force-displacement response of a sinusoidal elastica surrounded by an incompressible medium

The incompressibility assumption on the surrounding medium (Figure 6) leads to an explicit, simple expression for the value of the current amplitude of the sinusoidal elastica  $a(g)$ .

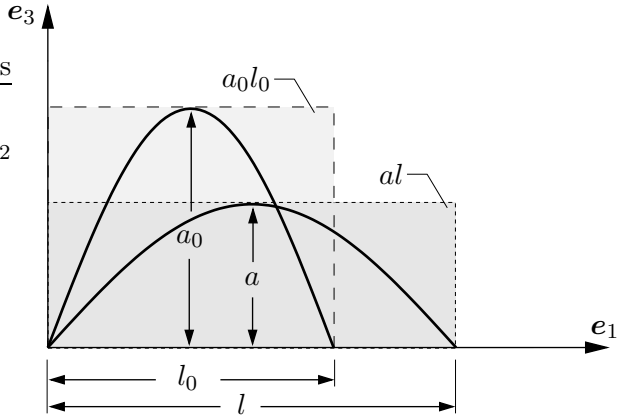


Figure 6: A sinusoidal elastica surrounded by an incompressible medium.

$$a_0 l_0 = a l \quad \rightsquigarrow \quad a(g) = \frac{a_0 l_0}{l} = \frac{a_0 l_0}{l_0 + g} \quad (35)$$

where  $a_0$  and  $l_0$  are the material parameters characterizing the initial shape of the crimp. Once the explicit form of the current amplitude  $a(g)$  in terms of the tip displacement  $g$  is known, the derivatives appearing in the integrand of the force expression (29) can be readily calculated

$$\frac{d\kappa}{dg} = \frac{3x_3''}{l} \frac{(x_3'^2-1)}{(1+x_3'^2)^{5/2}} \quad \text{and} \quad \frac{d\lambda^2}{dg} = \frac{2l}{l_0^2(1+X_3'^2)} \left( 1 + x_3'^2 \frac{l}{a} \frac{da}{dg} \right). \quad (36)$$

## 4.3 Force-displacement response of a sinusoidal elastica with stationary energy

The stationarity of energy is imposed with respect to the current amplitude  $a(g)$ , i.e.  $\partial_a \tilde{W}(g; a)\Big|_g = 0$ . This condition defines a non-linear residual  $\mathcal{R}(a)$

$$\mathcal{R}(a) := \int_0^{l_0} \left( B(\kappa - \kappa_0) \frac{\partial\kappa}{\partial a} + EA(\lambda^2 - 1) \frac{\partial\lambda^2}{\partial a} \right) J(t) dt. \quad (37)$$

that must vanish for a given tip displacement  $g$ . In (37), the functional dependencies  $\kappa = \hat{\kappa}(t, g; a(g))$  and  $\lambda = \hat{\lambda}(t, g; a(g))$  are suppressed. Equation (37) defines a non-linear residual. It is solved for  $a$  by a Newton-type iterative scheme.

With  $a$  being known the tip force,  $f$ , can be computed. Since the stationary energy condition requires that the partial derivative  $(\partial \tilde{W}(g; a)/\partial a)|_g$  vanishes, the terms contributing to the force quantity will be only the partial derivatives of kinematic variables with respect to the tip displacement  $g$ . That is, it suffices to compute the integrand terms

$$\frac{\partial \kappa}{\partial g} = \frac{x_3''}{l} \frac{(x_3'^2 - 2)}{(1 + x_3'^2)^{5/2}} \quad \text{and} \quad \frac{\partial \lambda^2}{\partial g} = \frac{2l}{l_0^2} \frac{1}{(1 + X_3'^2)}. \quad (38)$$

**Remark 1:** Consider the limiting case in which the tip displacement  $g$  is much larger than the initial half-wavelength  $l_0$ , i.e.  $g/l_0 \gg 1$ , and  $l/l_0 \approx g/l_0 \gg 1$ . In this condition the elastica is considerably straightened. Owing to the flat shape of the elastica, its spatial slope  $x_3'$  and the curvature  $x_3''$  are small. This implies that the contribution from the bending term to the overall tip force value in both (36)<sub>1</sub> and (38)<sub>1</sub> will be negligible in comparison with the contribution from the axial extension. Furthermore, the vanishing term  $x_3'$  in (36)<sub>2</sub> for large values of the tip displacement  $g$  makes the force terms in (36)<sub>2</sub> and (38)<sub>2</sub> tend toward each other. Then, provided the bending stiffness is not much larger than the axial stiffness, the tip force values for the incompressible bounding medium and stationary energy cases approach a common value at large tip displacement values.

**Remark 2:** All the models of the sinusoidal elastica discussed in the preceding Sections 4.1–4.3 apparently require an efficient numerical integration tool both for computing the tip force  $f$  and for carrying out the Newton-type iterations. For this purpose, we have employed a set of F77 subroutines, the so-called DCUHRE, providing a double precision adaptive integration tool which is based on the adaptive division of the integration domain into subregions. For the details of the theory and the implementation of the algorithm, the reader is referred to the articles by Berntsen et al. (1991a; 1991b).

## 5 Comparison of kinematic and constraint assumptions; validation

In the preceding Sections 2 and 4 the force–displacement formulation for the circular and sinusoidal elasticas has been outlined, respectively. Apart from the conservation of the selected shapes, three additional constraints have been considered for each shape. These are related to the kinematical, geometrical and energetic conditions that are specifically concerned with the inextensibility, incompressibility of the bounding medium and stationarity of energy. The present section is devoted to a comparative analysis of the force–stretch response of the circular and sinusoidal elasticas.

### 5.1 Comparison of the force-displacement response of circular-arc and sinusoidal elasticas subjected to different constraint conditions

We first consider the force–stretch behavior of the circular elastica subject to the three constraints. To this end, we make an assumption for the relation between the micro-tip displacement  $g$  and the macro-stretch  $\bar{\lambda}$ . The ratio between the ends of the elastica is assumed to be dictated by

macroscopic deformation in an affine manner. That is, the macro-stretch  $\bar{\lambda}$  is related to the tip displacement  $g$  by  $\bar{\lambda} := 1 + g/(2R)$ .<sup>1</sup> In the subsequent analyses the macro stretch will be used as the primary deformation variable controlling the process.

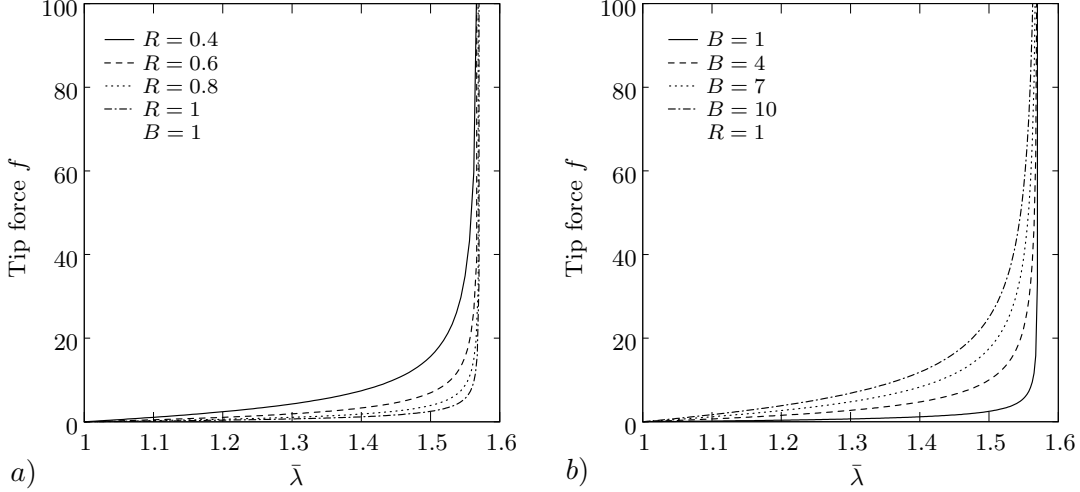


Figure 7: Circular inextensible elastica. Sensitivity analysis of the  $f - \bar{\lambda}$  curve to a) the variation of initial radius  $R \in [0.4, 1]$  and b) the variation of bending stiffness  $B \in [1, 10]$ .

For the circular, inextensible elastica, according to (10), the tip force  $f$  diverges as the tip displacement  $g$  approaches the value  $g_{max} = (\pi - 2)R$ . This implies that the maximum value of macro-stretch is  $\bar{\lambda}_{max} = \pi/2$ , as shown also in Figure 7. For the circular, inextensible elastica, the shape of the  $f - \bar{\lambda}$  curve depends only on the initial radius  $R$  and the bending stiffness  $B$ . Figures 7a and 7b clearly depict that the larger the initial radius  $R$  or the smaller the bending stiffness  $B$ , the sharper is the transition to the divergent behavior. Although the sharpness of the transition can be adjusted, the value of the locking stretch is always fixed to the value  $\bar{\lambda}_{max} = \pi/2$ . This considerably limits the ability to model a range of response functions with the circular inextensible elastica. It is particularly true from the viewpoint of matching experiments on different collagenous materials.

The sensitivity of the tip force,  $f$ , to the axial stiffness,  $EA$ , for  $B = 1$  and  $R = 1$  is depicted in Figure 8a for a circular elastica embedded in an incompressible medium. A decrease in the axial rigidity results in softening of the slope. Clearly, the axial rigidity dominates the stiffness of the  $f - \bar{\lambda}$  curve. The macroscopic stretch,  $\bar{\lambda}$  exceeds  $\bar{\lambda}_{max} = \pi/2$ . Observe that for increasing values of  $EA$ , the  $f - \bar{\lambda}$  curve approaches the behavior of the inextensible circular elastica (Figure 7). Although the variation in the axial stiffness provides flexibility in determining the shape of the curve, the incompressibility condition yields compression in the micro-stretch  $\lambda$ , which is probably spurious, for small  $\lambda$ . See Figure 8b. This drawback of the incompressibility constraint can also be demonstrated using the expression for  $\lambda$  given in (13). The influence of this non-physical outcome on the tip force diagram is non-convex behavior for small  $\bar{\lambda}$  as shown in Figure 8a. This disadvantage clearly restricts the use of this formulation.

The last case for the circular geometry is concerned with stationarity of energy. The material parameters used were the same as for the incompressible medium. As in the incompressible case

<sup>1</sup>For tissues with transverse isotropy, where the fibers (elastica) are characterized by end-to-end vectors that are highly aligned, affinity of deformation is a good assumption. The alternative, fiber slippage, will be treated in a separate paper.

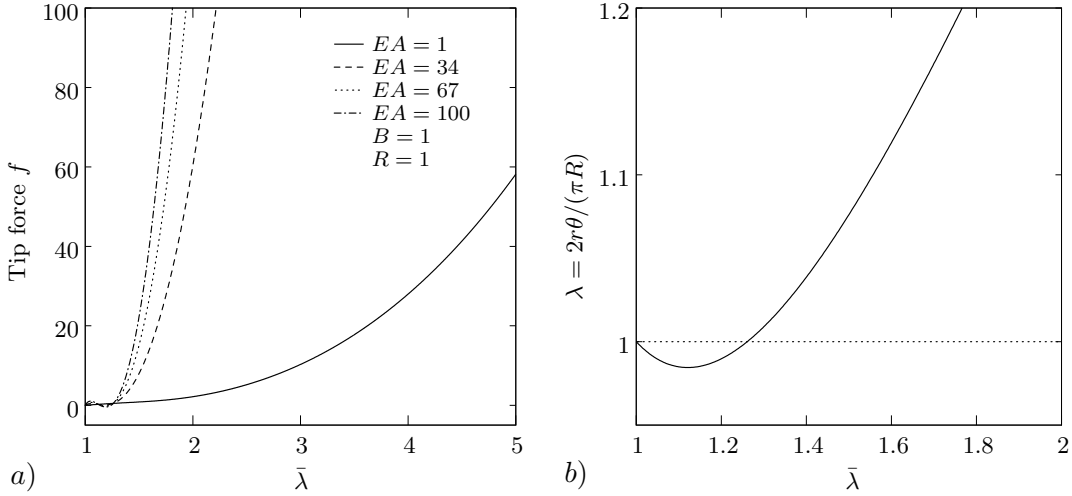


Figure 8: Circular elastica surrounded by an incompressible medium. a) Sensitivity analysis of the  $f-\bar{\lambda}$  curve to the variation of the axial stiffness  $EA \in [1, 100]$ . b) Micro-stretch  $\lambda$  vs. macro-stretch  $\bar{\lambda}$  curve.

a decrease in axial rigidity has a strong, depressing influence on stiffness of the  $f-\bar{\lambda}$  response. The elastica can be extended to  $\bar{\lambda} > \pi/2$ . With an increase in axial rigidity, the  $f-\bar{\lambda}$  curve approaches the behavior of the inextensible circular elastica (see Figure 9). Figure 10 compares all three cases of the circular elastica. Distinct values  $EA = 34, 67, 100$  are assigned to the axial modulus of the incompressible and stationary energy elastics. The  $f-\bar{\lambda}$  curve of the stationary energy case approaches the inextensible one by “rotating” about the “heel” just below  $\bar{\lambda}_{\max}$ . However, this occurs with no discernible difference in the curves for  $\lambda$  values smaller than the heel. In case of the elastica surrounded by an incompressible medium, however, the stiffening in the  $f-\bar{\lambda}$  behavior is different. Owing to the negative values of micro-stretch in the initial stages, the location of the heel is shifted to the smaller values of  $\bar{\lambda}$ .

In the foregoing parameter study, we solely considered the circular elastics with the different constraints describing its shape. In what follows, we present an analogous parameter sensitivity study for the sinusoidal geometry. In contrast to the circular elastica, the reference shape of a sinusoidal elastica is governed by two parameters: the amplitude  $a_0$  and the half-wave length  $l_0$  (see Figure 5). The order of the ratio of the amplitude to the half-wave length  $a_0/l_0$ , however, cannot be arbitrarily chosen. According to the measurement results reported by Dale et al. (1972), this ratio is measured to be limited to the values smaller than 0.1. Taking into account this fact in the subsequent analyses, the value of this ratio will be chosen to be  $a_0/l_0 < 0.2$ , which will allow us to consider values slightly larger than the experimental observations. Furthermore, analogous to the study on the circular elastics, the macro-stretch  $\bar{\lambda}$  will be considered as the primary deformation measure which is related to the tip displacement  $g$  by  $\bar{\lambda} := 1 + g/l_0$ .

First, we consider a sinusoidal elastica that is constrained to the global inextensibility condition given in (32). In Figure 11a the influence of the ratio  $a_0/l_0$  on the  $f-\bar{\lambda}$  curve is depicted. The value of  $a_0/l_0$  is increased from 0.05 to 0.2 while keeping the values of the material parameters fixed at  $B = 1$  and  $EA = 1$ . The effect of this ratio proves crucial in determining the value of stretch at which the heel occurs. The higher the ratio  $a_0/l_0$ , the longer the “toe” region preceding the heel. In other words, this parameter determines the value of  $\bar{\lambda}$  where the influence of the bending mechanism starts to diminish and the axial extension begins to govern the  $f-\bar{\lambda}$  curve. This stage of the curve is commonly called the *heel region* in the schematic description of the curve. In order

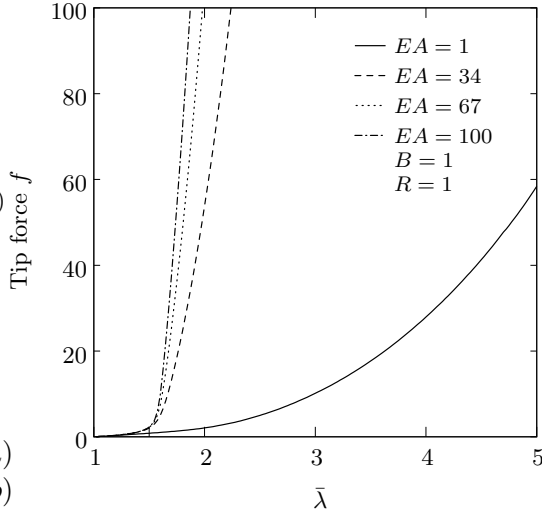


Figure 9: Circular elastica minimizing its energy. Sensitivity analysis of the  $f-\bar{\lambda}$  curve to the variation of the axial stiffness  $EA \in [1, 100]$ .

to show the sensitivity of the  $f-\bar{\lambda}$  curve to the bending stiffness, the ratio of bending stiffness to axial stiffness  $B/EA$  is varied from 1 to 4 (Figure 11b). An increase in the ratio  $B/EA$  scales the curve's ordinates ( $f$ -values), and therefore the transition in the heel region becomes more gradual. However, the value of the locking stretch is not influenced by the changes in the ratio  $B/EA$ .

In the last two cases we consider the incompressible and energy minimizing sinusoidal elasticas. Figures 12a and 13a present the influence of the change in ratio  $a_0/l_0$  on the  $f-\bar{\lambda}$  curves of the respective cases. Like the inextensible case the value of the ratio  $a_0/l_0$  is varied within the interval  $a_0/l_0 \in [0.05, 0.2]$  while the value of the ratio  $EA/B$  is kept frozen to the value 30. Clearly, the  $f-\bar{\lambda}$  curves for the incompressible and stationary energy cases do not exhibit a pronounced stiffening behavior. This is in contrast with the inextensible case, see Figure 11. Variation of the ratio  $a_0/l_0$  does not cause significant change in the shape of the curves.

The sensitivity of the  $f-\bar{\lambda}$  curves for the separate cases to changes in material parameters  $EA$  and  $B$  is presented in Figures 12b and 13b, respectively. The value of the ratio  $EA/B$  is increased from 30 to 300. The effect of the axial stiffening is reflected in the ordinates of the curves. No striking shape change is observed. It should be noticed that the  $f-\bar{\lambda}$  curves in Figures 12 and 13 for the incompressible and stationary energy cases of the sinusoidal elastica resemble each other. The quantitative reasoning for this observation has been already outlined in Remark 1.

## 5.2 Validation of constraint assumptions by numerical simulations

In the preceding section the sensitivities of the  $f-\bar{\lambda}$  curves to geometric and material parameters have been discussed for both the circular and the sinusoidal elasticas subjected to the three constraint conditions. In this section we carry out a comparison with data recently reported by Freed and Doehring (2005) (Figure 14). These data acquired correspond to uniaxial extension experiments on five chordae tendineae from porcine mitral valves. They demonstrate a long toe region relative to the maximum stretch in each experiment.. Beyond the heel region ( $\bar{\lambda} \approx 1.12$ ), the nominal stress-stretch curve is almost linear with a sharply larger slope. From the results in Figures 7–13 of the preceding parameter study, it is apparent that this behavior can only be captured either by the inextensible sinusoidal elastica, or the circular elastica attaining a stationary

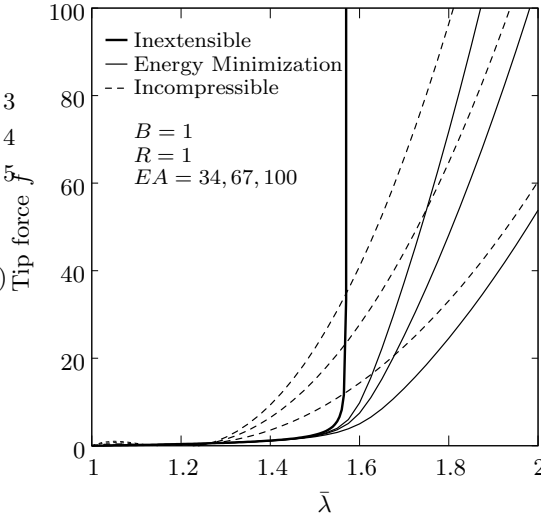


Figure 10: Comparison of circular elasticas subjected to different constraints. In the incompressible and energy minimization cases, three different values are assigned to the axial modulus  $EA = 34, 67, 100$ .

energy state. Figure 14a compares the experiment with these two models. Both the sinusoidal and the circular model successfully match the data in the toe region. The inextensible sinusoidal model can also predict the upturning region, but its stiffness beyond the heel region is much higher than the experiments indicate. The circular model, on the other hand, captures the stiffness of the post-heel region but the stretch value where the upturning takes place is over estimated. In order to highlight this fact, the stretch value (abscissa) of the simulation data by the circular elastica is scaled, i.e.  $\bar{\lambda}_{mod} = fact \cdot \bar{\lambda}$  and replotted in Figure 14b.

## 6 Macroscopic material model incorporating the elastica

### 6.1 Continuum strain energy functions at the macroscale

The contribution to the overall strain energy function per unit reference volume due to the collagen fibrils embedded in a nearly incompressible viscous medium is obtained by summing up the free energies of individual elasticas

$$\Psi_{col} = \frac{N}{A_0 l_0} \widetilde{W}(g). \quad (39)$$

With the unit vector  $\mathbf{e}$  denoting the average orientation of collagen fibrils, the macroscopic stretch in this direction is obtained by  $\bar{\lambda} = |\mathbf{F}\mathbf{e}|$ , where  $\mathbf{F}$  is the deformation gradient tensor. In the context of anisotropic elasticity, especially transverse isotropy, it is common to define structural tensors  $\mathbf{M} := \mathbf{e} \otimes \mathbf{e}$  for the construction of strain energy functions formulated in terms of additional invariants. The derivatives of these invariants are then used as tensor generators in the stress response functions. In the present case,  $I_4 := \mathbf{C} : \mathbf{M} = \bar{\lambda}^2$  is the relevant invariant ( $\mathbf{C}$  being the right Cauchy-Green tensot) if we assume an affine relation between the macro- and micro-stretches, i.e.  $\bar{\lambda} = (l_0 + g)/l_0$ . With this relation in hand, the contribution to the total second Piola-Kirchhoff stress tensor due to the stretching of collagen fibers  $\mathbf{S}^{col} = 2\partial_{\mathbf{C}}\Psi_{col}$  can be obtained as

$$\mathbf{S}^{col} = N \frac{f(g)/\bar{\lambda}}{A_0} \mathbf{M} \quad (40)$$

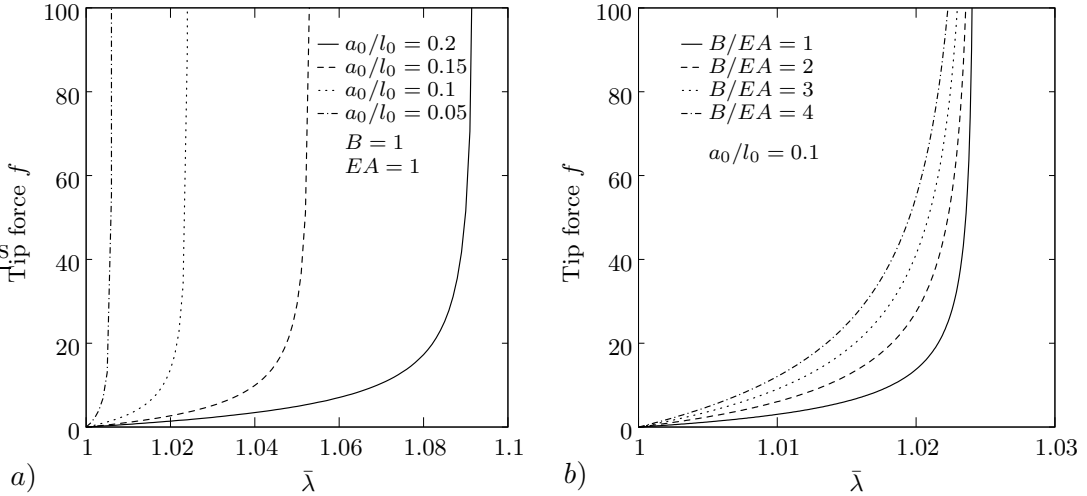


Figure 11: Comparison of the  $f-\bar{\lambda}$  curves for globally inextensible sinusoidal elasticae having different a)  $a_0/l_0$  and b)  $B/EA$  ratios.

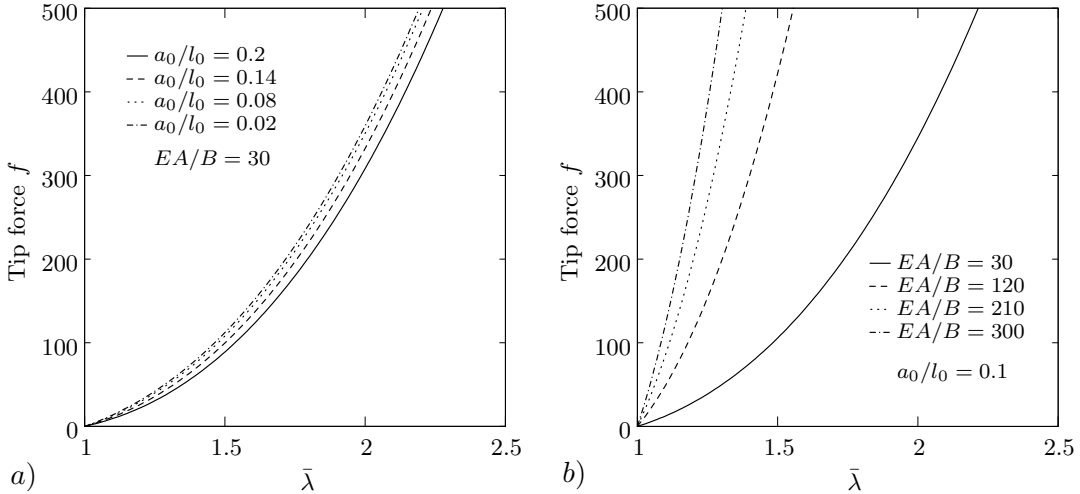


Figure 12: Comparison of the  $f-\bar{\lambda}$  curves for sinusoidal elasticae surrounded by an incompressible medium having different a)  $a_0/l_0$  and b)  $EA/B$  ratios.

where the results  $\partial g/\partial \bar{\lambda} = l_0$ ,  $2\partial \bar{\lambda}/\partial I_4 = 1/\bar{\lambda}$ ,  $\partial I_4/\partial \mathbf{C} = \mathbf{M}$  and the definition  $f(g) := d\widetilde{W}/dg$  have been used. Then, the nominal stress tensor  $\mathbf{P}^{\text{col}}$  readily follows  $\mathbf{P}^{\text{col}} = \mathbf{F}\mathbf{S}$

$$\mathbf{P}^{\text{col}} = N \frac{f(g)}{A_0} \tilde{\mathbf{e}} \otimes \mathbf{e} \quad (41)$$

where  $\mathbf{F}\mathbf{e} = \bar{\lambda}\tilde{\mathbf{e}}$  and  $|\tilde{\mathbf{e}}| = 1$ .

We now turn attention to the convexity of the strain energy  $\Psi_{\text{col}} = \hat{\Psi}_{\text{col}}(I_4)$ , in order to have a basic understanding of its stability properties. The convexity condition demands the positive definiteness of the first elasticity tensor  $\mathbb{A}^{\text{col}}$

$$\mathbf{H} : \mathbb{A}^{\text{col}} : \mathbf{H} \geq 0 \quad \forall \mathbf{H} \in \mathbb{M}^{3 \times 3} \quad \text{and} \quad \mathbb{A}^{\text{col}} := \frac{\partial^2 \hat{\Psi}_{\text{col}}}{\partial \mathbf{F} \partial \mathbf{F}}. \quad (42)$$

where  $\mathbb{M}^{3 \times 3}$  is the space of second-order tensors in  $\mathbb{R}^3$ .

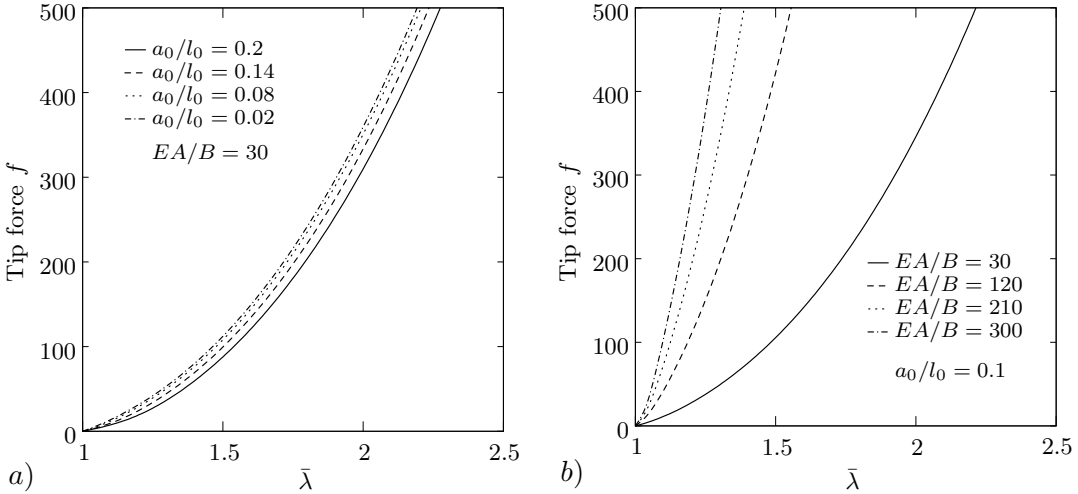


Figure 13: Comparison of the  $f-\bar{\lambda}$  curves for sinusoidal elasticas deforming by attaining stationary energy states for different a)  $a_0/l_0$  and b)  $EA/B$  ratios.

The explicit form of the first elasticity tensor  $\mathbb{A}^{\text{col}}$  can be obtained through chain rule operations as

$$\mathbb{A}^{\text{col}} := \hat{\Psi}'_{\text{col}} \frac{\partial^2 I_4}{\partial \mathbf{F} \partial \mathbf{F}} + \hat{\Psi}''_{\text{col}} \frac{\partial I_4}{\partial \mathbf{F}} \otimes \frac{\partial I_4}{\partial \mathbf{F}}. \quad (43)$$

Forming the quadratic product of  $\mathbb{A}^{\text{col}}$  with  $\mathbf{H}$  involves the terms

$$\mathbf{H} : \frac{\partial^2 I_4}{\partial \mathbf{F} \partial \mathbf{F}} : \mathbf{H} = 2|\mathbf{H}\mathbf{e}|^2 \geq 0, \quad \left( \frac{\partial I_4}{\partial \mathbf{F}} : \mathbf{H} \right)^2 = (\mathbf{H}\mathbf{e} \cdot \mathbf{F}\mathbf{e})^2 \geq 0 \quad (44)$$

both of which are positive. The local convexity condition (42) of the free energy  $\hat{\Psi}_{\text{col}}$  then reduces to

$$2\hat{\Psi}'_{\text{col}} |\mathbf{H}\mathbf{e}|^2 + 4\hat{\Psi}''_{\text{col}} (\mathbf{H}\mathbf{e} \cdot \mathbf{F}\mathbf{e})^2 \geq 0. \quad (45)$$

Based on (44), the positiveness of both  $\hat{\Psi}'_{\text{col}}$  and  $\hat{\Psi}''_{\text{col}}$  is sufficient to fulfill the convexity condition (45), though not necessary. The explicit forms of the derivatives are  $\hat{\Psi}'_{\text{col}} = Nf(g)/(2A_0\bar{\lambda})$  and  $\hat{\Psi}''_{\text{col}} = Nl_0(f'(g)l_0 + gf'(g) - f(g))/(4A_0\bar{\lambda}^2(g + l_0))$ . If we assume that collagen fibrils can carry only tensile loads, i.e. tension only elasticas, the positiveness of  $\hat{\Psi}'_{\text{col}}$  is satisfied identically for  $f(g) \geq 0$ . Furthermore, the convexity of  $\hat{\Psi}_{\text{col}}$  with respect to  $g$  ensures that  $f'(g) \geq 0$ . Thus, it is now sufficient to show that the term  $gf'(g) - f(g) \geq 0$  in  $\hat{\Psi}''_{\text{col}}$ . This condition can be obtained starting from the convexity condition for  $f(g)$  with respect to  $g$ , i.e.  $f''(g) \geq 0$ . For positive values of  $g$ , we have  $gf''(g) \geq 0$ . Integration of  $gf''(g) \geq 0$  by parts yields  $\int_0^g gf''(g) = gf'(g)|_0^g - \int_0^g f'(g) \geq 0$ . For  $f(0) = 0$ , we obtain the sought form  $gf'(g) - f(g) \geq 0$ . Therefore, convexity of both the  $\tilde{W}$  and  $f(g) = d\tilde{W}/dg$  guarantees the local convexity of the macroscopic free energy function  $\hat{\Psi}_{\text{col}}$ .

## 7 Closing remarks

The primary goal of this paper is to establish that the typical locking behavior seen in soft tissue such as tendons can be rigorously modelled by the energetically-based response of collagen fibrils. While entropic elasticity-based models can also model the locking behavior, there are strong physical and physiological reasons to surmise that this is the wrong approach to adopt. The energetic elasticity

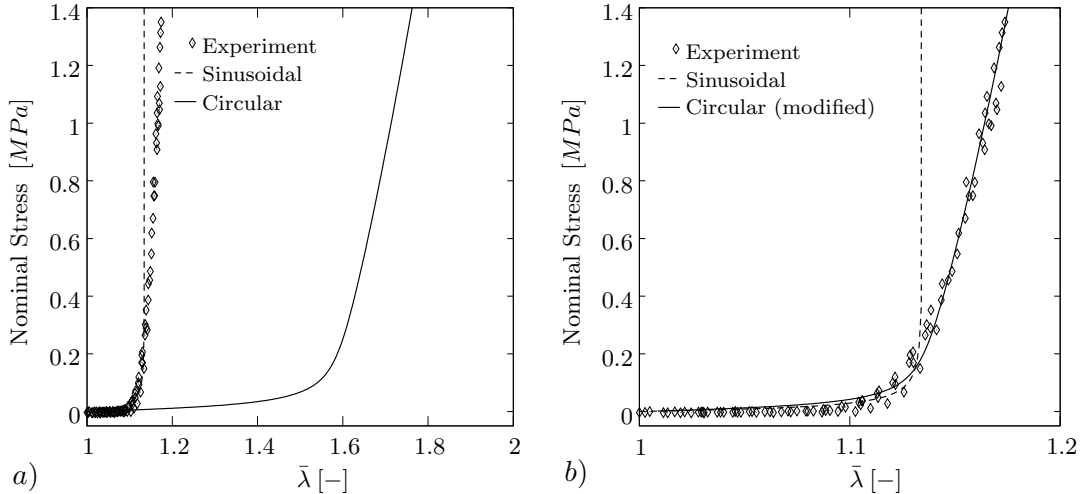


Figure 14: Simulations of the experimental data by the inextensible sinusoidal elastica ( $a_0/l_0 = 0.245$ ,  $B/EA = 30$ ) and the circular elastica minimizing its energy ( $r_0 = 0.013$ ,  $B/EA = 6.25/3 \cdot 10^{-6}$ ).  $r_0, a_0$  and  $l_0$  are in  $mm$  and  $B, EA$  are in  $MPa$ .

of fibrils is based on the response of a deforming elastica. The direct solution of the shape and force generated by a deforming elastica requires the solution of a (“highly”) nonlinear, fourth-order partial differential equation. The simplification advanced here is that judiciously-chosen constraints, kinematic and otherwise, can lead to force-deformation response functions for the elastica. Beyond this, the paper is concerned with an enumeration of two families of shapes (circular arcs and sinusoidal half-periods) of the deforming elastica, and three possible additional constraints. These additional constraints: inextensibility, macroscopic incompressibility, and stationarity of energy are well-founded in a physical sense. Their suitability in matching a set of experimental force-deformation curves has been examined. On the basis of the current limitation to elastic effects, it emerges that the elastica deforming as a circular arc, and maintaining itself in a state of stationary energy in each configuration (parametrized by overall elongation) best resolves the experimental data. The importance of inelastic effects such as the viscous friction as fibrils move relative to the surrounding proteoglycans, viscoelasticity of the proteoglycans themselves, and slippage of fibrils under larger forces, must not be overlooked, however.

It should also be quite clear, that the development here has complete relevance for any composite consisting of mainly unidirectional, elastica-like reinforcing fibers in a compliant matrix.

## References

- Berntsen, J., Espelid, T. O., Genz, A., 1991a. An adaptive algorithm for the approximate calculation of multiple integrals. *ACM Transactions on Mathematical Software* 17 (4), 437–451.
- Berntsen, J., Espelid, T. O., Genz, A., 1991b. Algorithm 698: Dcuhre: An adaptive multidimensional integration routine for a vector of integrals. *ACM Transactions on Mathematical Software* 17 (4), 452–456.
- Dale, W. C., Baer, E., Keller, A., Kohn, R. R., 1972. On the ultrastructure of mammalian tendon. *Experientia* 28, 1293–1295.

- Freed, A. D., Doehring, T. C., 2005. Elastic model for crimped collagen fibrils. *ASME Journal of Biomechanical Engineering* 127, 587–593.
- Holzapfel, G. A., Ogden, R. W., 2006. *Mechanics of Biological Tissue*. Springer Verlag.
- Kratky, O., Porod, G., 1949. Röntgenuntersuchungen gelöster Fadenmoleküle. *Recueil Trav. Chim* 68, 1106–1122.
- Landau, L. D., Lifshitz, E. M., 1951. *A Course on Theoretical Physics, Volume 5, Statistical Physics, Part I*. Butterworth Heinemann (reprint).
- Provenzano, P. P., Vanderby, R., 2006. Collagen fibril morphology and organization: Implications for force transmission in ligament and tendon. *Matrix Biology* 25, 71.
- Screen, H. R. C., Lee, D. A., Bader, D. L., Shelton, J. C., 2003. An investigation into the effects of the hierarchical structure of tendon fascicles on micromechanical properties. *Proc. Instn. Mech. Engr* 218, 109.
- Sun, Y.-L., Luo, Z.-P., Fertala, A., An, K.-N., 2002. Direct quantification of the flexibility of type I collagen monomer. *Biochemical and Biophysical Research Communications* 4295, 382–386.
- Treloar, L. R. G., 1975. *The physics of rubber elasticity*. Oxford Clarendon Press.
- Woo, S. L.-Y., Lee, T. Q., Gomez, M. A., Sato, S., Field, F. P., 1987. Temperature-dependent behavior of the canine medial collateral ligament. *J. Bio. Mech. Engrg. Trans ASME* 109, 68.